

Research Article

Behavior of Fibrous Hollow Reinforced Concrete Beams

Nasr Z. Hassan, Hala M. Ismael and Amany M. Salman*

Civil Engineering Department, Helwan University, Cairo, Egypt

Received 02 Oct 2018, Accepted 05 Dec 2018, Available online 07 Dec, Vol.8, No.6 (Nov/Dec 2018)

Abstract

Based on the experimental result of eight hollow reinforced concrete beams, an experimental program is carried out to study behavior of the same beams but with adding 0.75% steel fiber content by volume to concrete mix. The tested hollow beams without steel fiber exhibited lower shear resistance and wider cracks when compared to solid beam. Eight beams had the same size of 2500mm x 200mm x 300mm were casted and tested under four point bending test. The results show that adding steel fibers to concrete mix optimize the mechanical properties for all hollow beams as steel fibers inhibit cracking process and increase fracture energy. All beams with steel fibers had higher load carrying capacity ranging from 3.64% to 24.73% than those without steel fiber. The inclusion of steel fibers enhanced ductility index and absorbed energy and made the reinforced concrete sections to behave in a ductile manner. ANSYS (14.5) finite element program was used to simulate the behavior of all tested beams. The steel fibers were assumed as smeared reinforcement layers embedded in SOLID65 elements. Modeling element by FE program saving time and cost.

Keywords: Steel Fiber Reinforced Concrete (SFRC), Hollow beams, PVC pipe, Finite Element Analysis (FEA), ANSYS.

1. Introduction

At last years, many research indicated that adding steel fibers to concrete structures improve its performance where concrete is a brittle material with low tensile strength. The main benefit of fibers is their ability to transfer stresses across a crack, enhancing the toughness and ductility of the concrete as well as the absorption capacity under impact (Clarke, Vollum *et al.* 2007).

Steel fiber reinforced concrete (SFRC) is concrete made of hydraulic cements containing fine and coarse aggregate and discontinuous discrete steel fibers. In tension, (SFRC) fails only after the steel fiber breaks or is pulled out of the cement matrix. This happening depends on bond strength of the matrix. Fiber pull-out is more desirable as it makes the SFRC more ductile with absorbing a greater amount of energy (Netra B. Karki, 2011). SFRC has been used in construction of industrial floors, bridge deck overlays, highway pavements, airport runways, spillways, tunnel linings, dams, slope stabilizations and other precast products. In early period of 1950 and 1960, the conventional fibers used in (FRC) were straight and smooth. In order to improve mechanical bonding with cement matrix fibers with more complicated geometries have been developed. Fibers which have larger surface area to volume ratio can have higher bond strengths. Figure.1 shows various geometries of the steel fibers used in SFRC (ACI 544.1R, 1996).

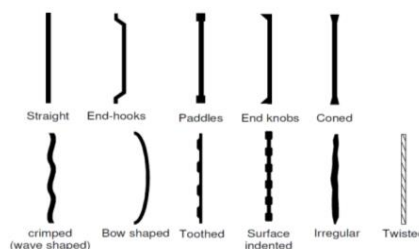


Fig.1 Geometries of Steel Fibers (ACI 544.1R, 1996)

(ACI 544.1R, 1996) also stated that, steel fibers used in SFRC should be short, having an aspect ratio (ratio of length to diameter) from about 20 to 100, with any of shown cross-sections, and that are sufficiently small enough to be randomly dispersed in an unhardened concrete mixture using usual mixing procedures.

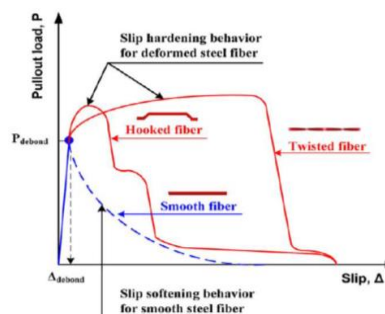


Fig. 2 Different Pullout Mechanisms according to Geometry of Steel Fiber (Kima *et al*, 2013)

*Corresponding author's ORCID ID: 0000-0001-6110-6966
DOI: <https://doi.org/10.14741/ijcjet/v.8.6.13>

(J. J Kima, D. J Kima, Kangb, & Lee 2013) proved that deformed hooked and twisted steel fiber produced much higher interfacial bond strength than smooth steel fiber as shown Figure 2.

This paper is part of research about optimizing hollow reinforced concrete beams. The crimped steel fiber with 0.75% volume fraction has been used in the present experimental study.

2. Objective of the Work

Based on results of tested hollow reinforced concrete beams (Nasr, Hala & Amany, 2019) the main drawback was the brittle shear failure due to lack of resistance shear area. By adding steel fibers to hollow reinforced concrete beams the shear strength will increased and failure mode change to a more ductile one. This paper aims to optimize behavior of hollow reinforced concrete beams through studying experimentally and analytically effect of adding 0.75% steel fiber content on beams with following parameters:

1. Tension reinforcement ratio (0.010 and 0.018)
2. Diameter of PVC pipe (50mm and 75mm)
3. Center position of PVC pipe from the top of section (160mm and 180mm)
4. Simulate and analysis hollow SFRC using program ANSYS 14.5

3. Review on Mechanical Properties of SFRC

Steel fibers improve the ductility of concrete under all modes of loading, but their benefit in improving strength differs among compression, tension, shear, torsion, and flexure. Improvements in ductility depend on the type and volume percentage of fibers (ACI 544.1R, 1996).

3.1 In Compression

Referring to (Johnston, C.D, 1974) the ultimate strength is only slightly affected by the presence of fibers, with observed increases ranging from 0 to 15 % for up to 1.5 % by volume of fibers. However, the fibers do substantially increase in the post-cracking ductility, or energy absorption of the material as shown in Figure 3

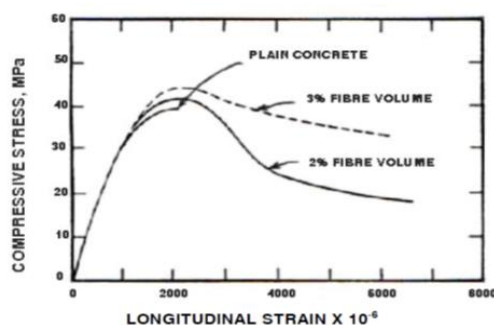


Fig. 3 Stress-Strain Curves in Compression for SFRC

(Thomas and Ramaswamy 2007) also stated that even with 1.5% of fibers the increase in peak strength was under 10% and the main role of steel fibers is only to reduce the rate of strength loss after the peak stress.

3.2 In Direct Tension

(ACI 544.1R, 1996) stated that, the improvement in strength is significant, with increases of 30% to 40 % for the addition of 1.5 % by volume of fibers in mortar or concrete. More about the tensile model of SFRC was discussed by (Naaman, 2008). As shown in Figure 4(a). The model generally consists of at two states. The first state is the pre-cracking state which is the elastic portion as shown in part I of Figure 4(b). The second state is the post-cracking state. This state consists of two phases. First phase of second state is the strain hardening with multi cracking phase as shown in Part II of Figure 4(b). This phase may not always exist as it depends on fiber types, fiber content and cement composites. Second phase of the post-cracking state involves the fiber pull-out or failure of fibers (Part III of Figure 4(b)).

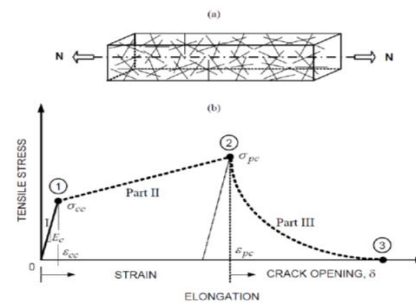


Fig.4 (a) Tensile Model with Discrete Fiber (b) Idealized Stress Strain Hardening of FRC Composite

The tensile stress in FRC composite just before the first cracking is given by:

$$\sigma_c = \sigma_f * Vf + \sigma_m * Vm \tag{1}$$

Where:

σ_f : Ultimate pullout strength of steel fiber (MPa)

σ_m : Ultimate tensile strength of un-cracked concrete matrix (MPa)

Vf : Volume fraction of fiber

Vm : Volume fraction of matrix (1 - Vf)

In case of SFRC when the concrete cracks, matrix attribution could neglect and the entire stress is carried by the fibers. Hence the ultimate tensile strength of the SFRC composite is given in terms of pullout strength of the fiber σ_f

$$\sigma_t = \sigma_f * Vf \tag{2}$$

And by applying effect of orientation, bond efficiency and length efficiency factors (Swamy *et al.*, 1974), the ultimate tensile strength of fiber reinforced concrete is given by:

$$\sigma t = 2 * \eta o * \eta b * \eta l * \tau * \frac{l_f}{d_f} * Vf \tag{3}$$

$$\tau = 0.66 * \sqrt{f_c} \tag{4}$$

Where:

- ηo : Orientation factor (0.405)
- ηb : Bond efficiency factor depending upon the fiber shape (1.2 for crimped fiber)
- $\frac{l_f}{d_f}$: Length of fiber to diameter of fiber in (mm)
- τ : Bond strength between fiber and matrix
- f_c : Compressive strength of normal concrete
- ηl : Length correction factor

$$\eta l = 1 - \frac{\tanh(\beta * \frac{l_f}{2})}{(\beta * \frac{l_f}{2})}$$

Where: l_f is the fiber length and β is factor determined by:

$$\beta = \sqrt{\frac{2 * \pi * Gm}{Ef * Af * Ln(\frac{S}{l_f})}} \rightarrow S = 25 * \sqrt{\frac{d_f}{Vf * l_f}} \tag{5}$$

Where: Gm is matrix shear modulus Af is fiber cross-sectional area and S is the mean centroid spacing in mm.

3.3 Shear and Torsion

Steel fibers generally increase the shear and torsional strength of concrete. For 1% by volume of fibers, the increases in shear range from negligible to 30 % (Barr, B, 1987). More recently (Hai H. Dinh, 2009) have concluded that using steel hooked-end fibers in a volume fraction greater than or equal to 0.75% leads to a significant increase of shear strength of concrete beams. Also a new provision by (ACI-318, 2014) allowed steel fibers as alternate shear reinforcement, if a minimum amount volume fraction of 0.75% is used.

3.4 Flexural Toughness and Flexural Strength

Under static loading, flexural toughness may be defined as the area under the load versus deflection curve which is the total energy absorbed to complete separation of the specimen (ACI 544.1R, 1996). Load versus deflection curves for concrete with different types and amounts of fiber are shown in Figure 5 and illustrated that enhancement in flexural toughness for all specimens with steel fiber when compared to control specimen (fibers make the material to have load-carrying capacity in the post-peak region).

(Ashour, Wafa, and Kamal, 2000) reported that Flexure capacity enhancement was 7.52% and 26.43% respective to 0.50 % and 1.00 % of fiber content. Also (Thomas and Ramaswamy, 2007) used hooked steel fibers with different steel fiber volume fraction ranging between 0.50% to 1.50% and recorded increasing in first crack flexural strength up to 40.00%.

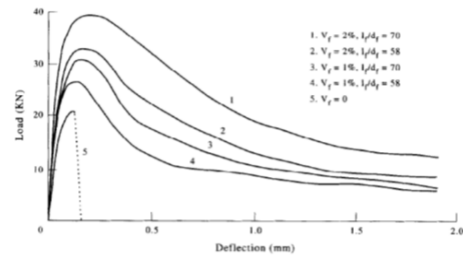


Fig. 5 Typical Flexural Load-Deflection Curves of SFRC (Gao et al, 1997)

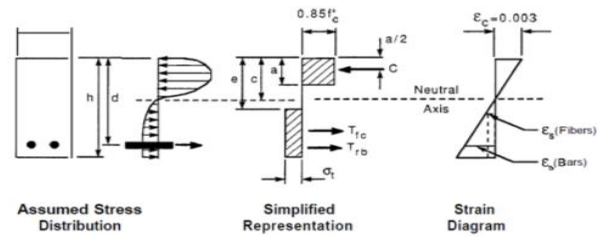


Fig. 6 Design Assumptions for Analysis of Singly Reinforced Concrete Beams Containing Steel Fibers

(Henager & Doherty, 1976) developed a method for predicting the strength of beams reinforced with both bars and fibers. The basic design assumptions are shown in Figure 6 and the equation for nominal moment M_n of a singly reinforced steel fibrous concrete beam is:

$$Mn = As * Fy * \left(d - \frac{a}{2}\right) + \sigma t * b * (h - e) * \left(\frac{h}{2} + \frac{e}{2} - \frac{a}{2}\right) \tag{6}$$

$$\sigma t = 0.00772 * Vf * Fbe * \frac{l}{a} \text{ N/mm}^2 \tag{7}$$

$$e = \left(\frac{\epsilon_f + 0.003}{0.003}\right) * c \tag{8}$$

$$\epsilon f = \frac{\sigma f}{Ef} \rightarrow \sigma f = \tau * \frac{l_f}{d_f} \tag{9}$$

Where:

- Fbe : The bond efficiency factor of the fiber, which varies from 1.0 to 1.2
- a : The depth of the rectangular stress block
- b : The width of the beam
- d : The distance from the extreme compression fiber to the centroid of the tensile reinforcement
- e : The distance from the extreme compression fiber to the centroid of the tensile block of fibrous concrete
- As : The area of the tension reinforcement
- C : the compressive force
- h : The total depth of the beam
- Es : the modulus of elasticity of steel
- T_{fc} : the tensile force of the fibers concrete
- T_{rb} : the tensile force of the bar reinforcement

3.5 Bond Performance

(Cairns & Plizzari, 2004) mentioned that fibers contribute to bond through two mechanisms: by confining reinforcement and by widening the range of

crack width values this confinement remains activated. As well as the main action of fibers related bond is that they improve considerably the ductility of bond failure, and this is so even for low fiber contents.

4. Material and Experimental Program

4.1 Materials

The materials used in this experimental work are local materials and agree with (ECP 203, 2017) limits (sand, gravel, ordinary Portland cement and drinking water). All batches used were of good quality, clean and free from organic material as shown in Figure 7. Two diameters (50mm and 75mm) of PVC pipe were used only to make longitudinal hollow in tested beams.



Fig. 7 Cement, Gravel and Sand Used in Experimental Work

Crimped (corrugated) steel fibers with 0.75% volume fraction were used with length 50mm, diameter 1mm having aspect ratio ($l/d = 50$), density of about 7800 kg/m³, tensile strength 1050MPa and modulus of elasticity 200GPa as shown in Figure 8.



Fig. 8 Steel Fibers and PVC Pipe Used in Experimental Work

The compressive strength of tested concrete cube with 0.75% steel fiber volume fraction was a about 34.00MPa after 28 days and the split tensile strength was about 4.00MPa. Figure 9 shows shape of cube with and without steel fiber under compression test machine and Figure 10 shows shape of cylinder with and without steel fiber to estimate spilt tensile

strength. The mix design of used concrete had the following composition per 1-meter cube in Table1. The main longitudinal reinforcement had yield stress of 400MPa, and stirrups had yield stress of 240MPa



Fig.9 Concrete Cube Compressive Strength Test. (A) without Steel Fiber (B) with Steel Fiber

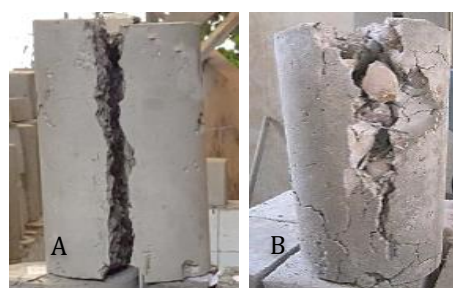


Fig.10 Concrete Cylinder Splitting Tensile Strength Test (A) without Steel Fiber (B) with Steel Fiber

Table 1 Mix Design for M34 Grade Concrete

Portland cement Kg/m ³	350
sand kg/m ³	800
gravel kg/m ³	1200
water kg/m ³	175
water cement ratio	0.50
Mix Ratio	1 : 2.28 : 3.42 : 0.50
Steel fiber kg/m ³	58.50

4.2 Experimental Program

Eight beams had the same concrete dimensions (2500mm x200mm x300mm) and the same top reinforcement 2Ø10 were casted and tested as shown in Figure 11. The tested beams divided in four groups according to diameter of PVC pipe used and their center position from the top of section as illustrated in Table 2.

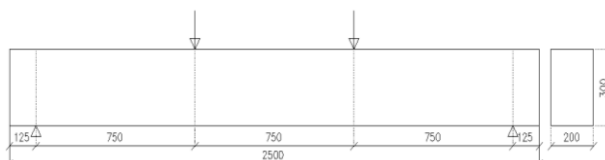


Fig. 11 Concrete Dimension

Table 2 Detailed Parameters of Tested beams

Group	Beam	PVC Diameter	PVC position	As	Stirrup/m
G.1	B-1-2	50mm	160mm	3Ø16	6Ø8
	B-1-4			5Ø16	10Ø8
G.2	B-2-2	50mm	180mm	3Ø16	6Ø8
	B-2-4			5Ø16	10Ø8
G.3	B-3-2	75mm	160mm	3Ø16	6Ø8
	B-3-4			5Ø16	10Ø8
G.4	B-4-2	75mm	180mm	3Ø16	6Ø8
	B-4-4			5Ø16	10Ø8

The preparation of the reinforcement cages of the beams and hanging PVC pipes according to their center location are shown Figure 12

To measure the strain in tension bars and stirrups, electrical strain gauges with length 10mm were attached to the main reinforcing bars at flexural zone and 6mm were attached to stirrups at shear zone (located at 150 mm from left support). The steel strain was measured and recorded using digital strain indicator connected to data acquisition system. Figure 13 shows the fixing of the strain gauges to tension bar and stirrup and measuring its efficiency.

The reinforcing cages were placed in the wooden forms which coated with oil. Then Concrete was prepared in a tilting rotary drum mixer with adding 0.75% volume fraction of steel fiber and casted in the form. Electrical vibrator was used to compact concrete mechanically, Figure 14 shows mixing, casting and compacting of concrete. After three days the wooden forms were removed. Specimens were cured for 28 days through covering surface by water and sheets as shown in Figure 15.



Fig. 12 Reinforcing Cages and Holding PVC Pipes



Fig. 13 Fixing Strain gauge and measuring its Efficiency

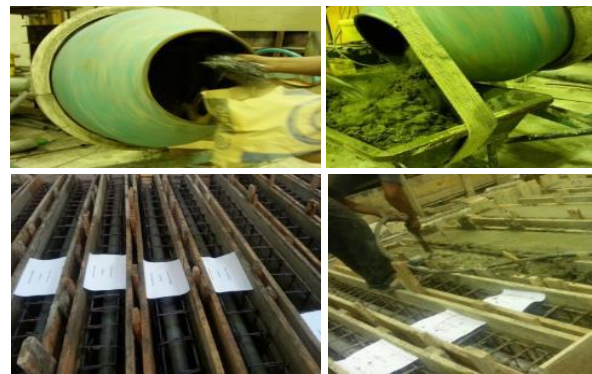


Fig. 14 Mixing, Casting and Compacting SFRC



Fig. 15 Curing of Cubes, Cylinder and Beam Specimens

4.3 Test Setup and Procedure

The beam testing frame of 500kN bearing capacity was used. The beams were tested under a two point loading system using a hydraulic jack attached to the loading frame. Three dial gauges were used to measure vertical deflection of the beams. The first one was located at the middle of the span and others under two points of loading. At the time of testing, the specimen was painted with white cement to help the visual crack detection during testing process. The load was applied gradually with constant rate and the readings of measurements devices were recorded in paper sheet at every increment of load. The cracking load was recorded once the first crack noticed. The specimen was loaded until reaching failure load. A data logger and a reader were used to measure strains in bars and loading values as shown in Figure 16



Fig. 16 Beam Test Setup, Dial Gauge and Load Cell

5. Experimental Results

5.1 Cracking Load and Ultimate Load

Table 3 and Table 4 clarify the experimental results of hollow SFRC beams and RC beams respectively. Including first cracking loads and corresponding deflections (P_{cr} and Δ_{cr}) also maximum loads and corresponding deflections (P_{max} and Δ_{max})

Table 3 Cracking and Ultimate Load of SFRC Beams

Group	Beam	P_{cr} (kN)	Δ_{cr} (mm)	P_{max} (kN)	Δ_{max} (mm)
G.1	B-1-2	73.70	3.37	221.90	16.92
	B-1-4	103.5	4.15	305.70	18.26
G.2	B-2-2	72.70	3.27	218.10	16.33
	B-2-4	123.5	4.18	320.70	18.62
G.3	B-3-2	58.70	2.11	241.00	18.22
	B-3-4	84.60	2.64	332.60	11.84
G.4	B-4-2	56.70	2.66	231.00	14.86
	B-4-4	80.60	2.69	314.70	15.38

Table 4 Cracking and Ultimate Load of RC Beams

Group	Beam	P_{cr} (kN)	Δ_{cr} (mm)	P_{max} (kN)	Δ_{max} (mm)
G.1	B-1-1	71.70	2.82	214.10	13.33
	B-1-3	84.60	2.56	260.0	11.53
G.2	B-2-1	68.70	2.43	209.10	9.78
	B-2-3	78.60	2.40	277.8	17.02
G.3	B-3-1	45.80	1.65	224.10	16.98
	B-3-3	72.70	2.19	273.00	11.84
G.4	B-4-1	46.80	1.76	185.20	12.79
	B-4-3	67.70	2.15	257.90	11.09

By comparing results it was found that:

1. For under reinforced section the first cracking loads and ultimate load of hollow SFRC beams increased than RC beams without steel fiber by percentage (28.16%) and (16.14%) respectively.
2. For over reinforced section the first cracking loads and ultimate load of hollow SFRC beams increased than RC beams without steel fiber by percentage up to (57.12%) and (35.96%) respectively

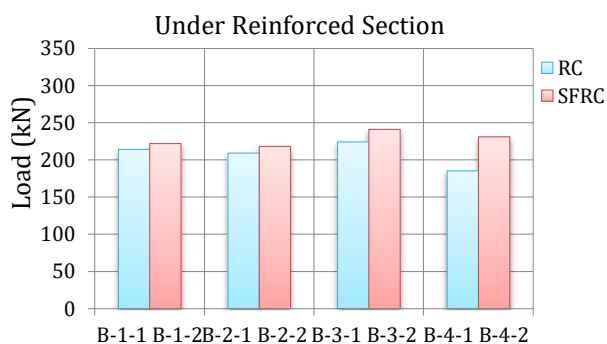


Fig.17 Comparing Ultimate Load for RC and SFRC Beams with Under Reinforced Section

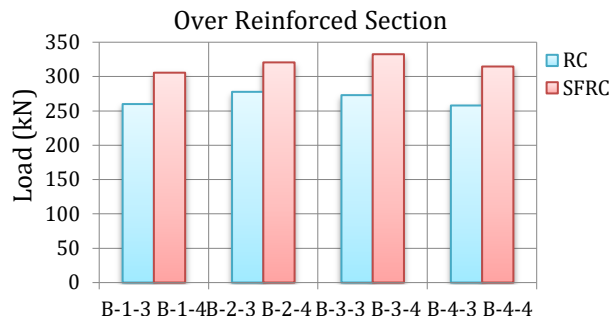


Fig.18 Comparing Ultimate Load for RC and SFRC Beams with Over Reinforced Section

5.2 Load Deflection Curves

The load deflection curves of tested beams with under reinforced sections and over reinforced sections for point at the mid span are shown in Figure 19 and Figure 20 respectively.

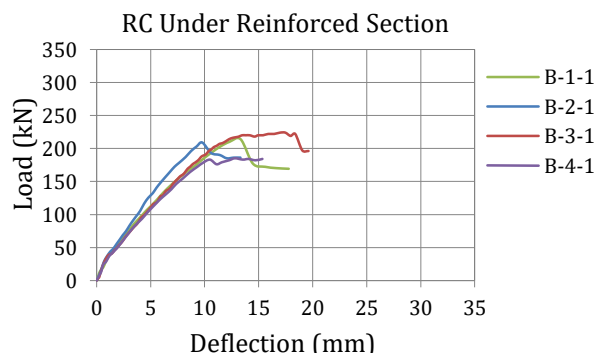
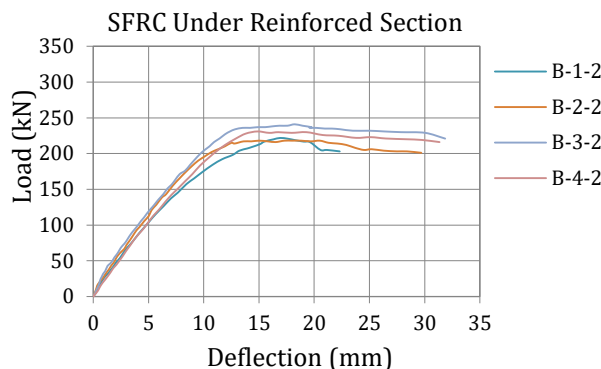


Fig. 19 Load-Deflection Curves for Under Reinforced Beams with and without Steel Fiber

From figures 19 and figure 20, adding steel fiber make the beam to have load-carrying capacity in the post-peak zone through reduce the rate of strength loss after the peak stress especially for beams with under reinforced section this is due to reaching concrete and steel to their max strengths then higher number of cracks formed allowing to more steel fiber attribute in bridging cracks so a considerable ductility and absorbed energy achieved.

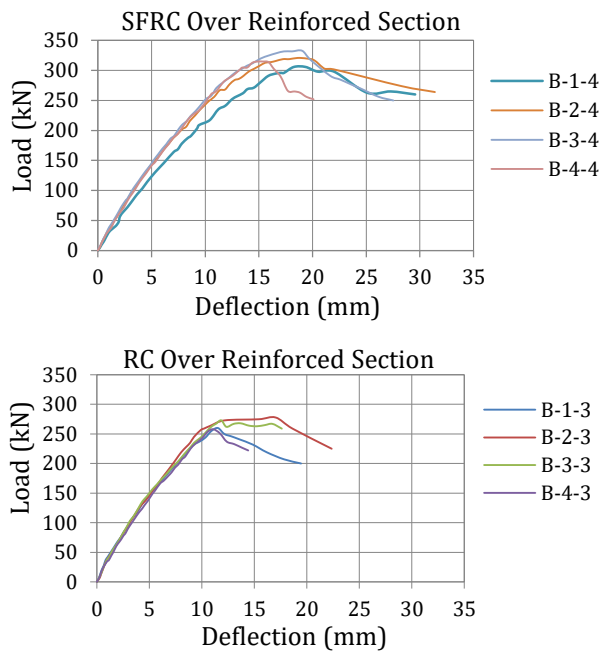


Fig. 20 Load-Deflection Curves for Over Reinforced Beams with and without Steel Fiber

5.3 Cracks Development and Failure Mode

Figure 21 and Figure 22 show crack patterns for hollow SFRC beams with under reinforced sections and over reinforced section respectively.

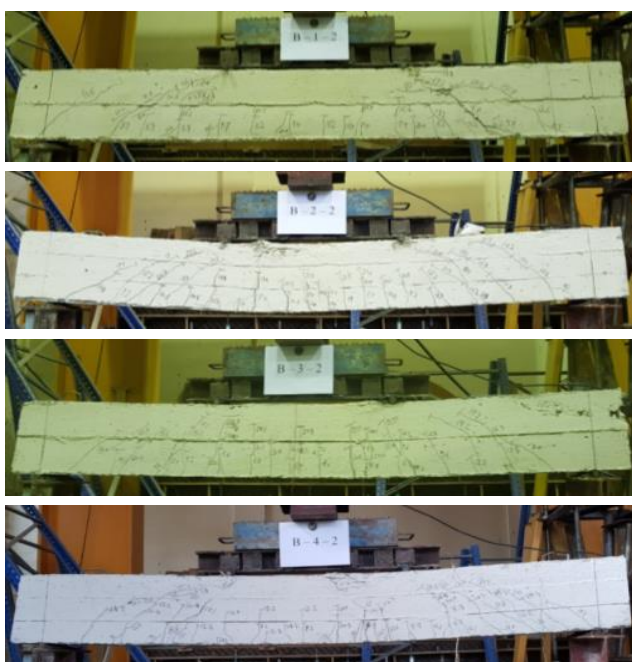


Fig.21 Crack Pattern for SFRC Beams with Under Reinforced Section

From figure 19 and figure 20, all the SFRC hollow beams had the same failure procedure. The main procedure can be illustrated as follows: the cracks of hollow SFRC tested beams started within the two

loading points. As load increased smaller crack formed in shear zone and widened slowly due to steel fiber bridging action where energy is dissipated through the deboned of the matrix and fiber pull-out. At failure, the diagonal shear cracks extended till the loading point, the concrete in the compression zone crushed and cracks at flexural zone continued to widen as the load increased causing flexural failure. Including steel fiber limited sudden brittle shear failure for most of hollow under reinforced section but for hollow over reinforced section the hollow beam with smaller PVC pipe diameter 50mm the failure mode changing to flexural one and hollow beam with larger PVC pipe diameter 75mm had shear failure but the beams became tougher and more ductile with smaller crack width.

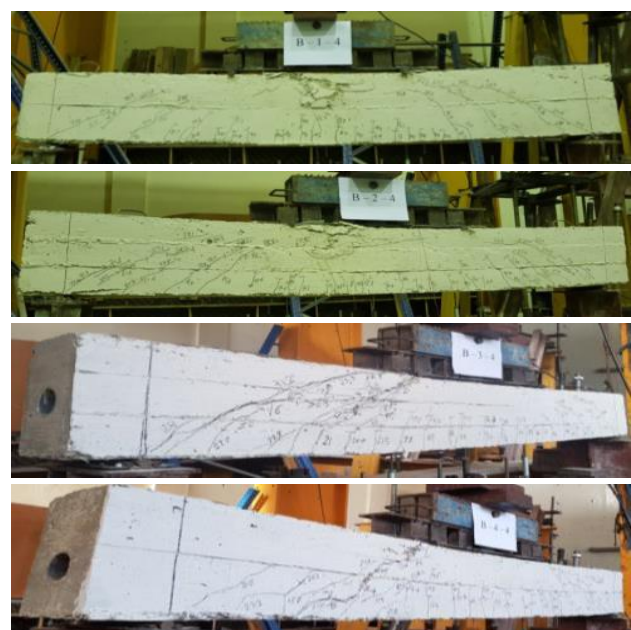


Fig.22 Crack Pattern for SFRC Beams with Over Reinforced Section

5.4 Strains in Tension Reinforcement and Stirrup

Table 4 illustrates values of maximum strain in tension bars and stirrups (ϵ_1 and ϵ_2 respectively) and failure mode for all hollow SFRC tested beams.

Table 4 Maximum Values of Strain in Tension Bars and Stirrups with Failure Type for Each Hollow SFRC Beam

Group	Beam	$\epsilon_1/10^6$	$\epsilon_2/10^6$	Failure type
G.1	B-1-2	2976	-----	Shear
	B-1-4	3842	2860	Flexural
G.2	B-2-2	3529	-----	Flexural
	B-2-4	3359	1321	Flexural
G.3	B-3-2	3564	856	Flexural
	B-3-4	3966	1260	Shear
G.4	B-4-2	3847	1469	Flexural
	B-4-4	3368	753	Shear

The relation between the strain of tension bar and the applied load for under reinforced beams and over reinforced beams with and without steel fiber are shown in Figure 23 and Figure 24 respectively. And the relation between the strain of stirrups and the applied load for under reinforced beams and over reinforced beams with and without steel fiber are shown in Figure 25 and Figure 26 respectively.

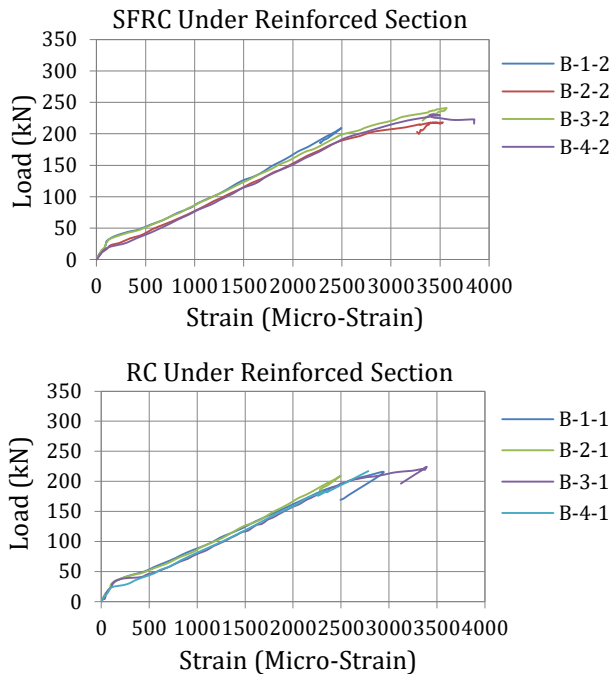


Fig.23 Load-Strain Curves of Tension Bar for under Reinforced Beams with and without Steel Fiber

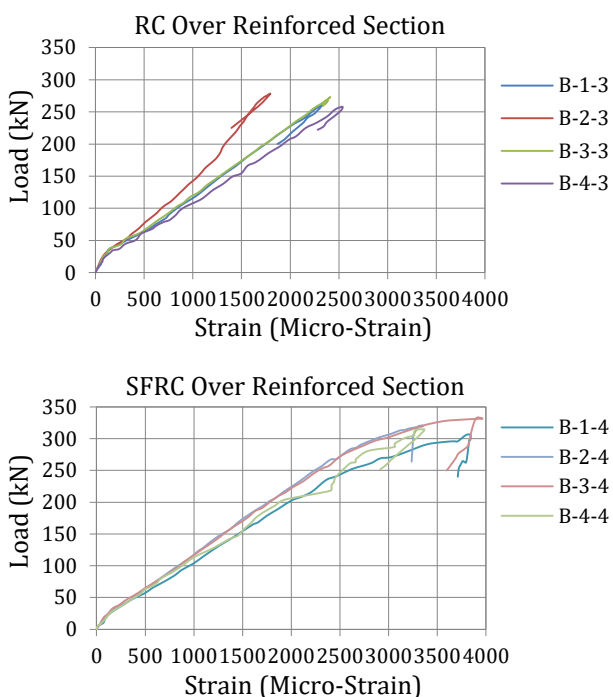


Fig.24 Load-Strain Curves of Tension Bar for over Reinforced Beams with and without Steel Fiber

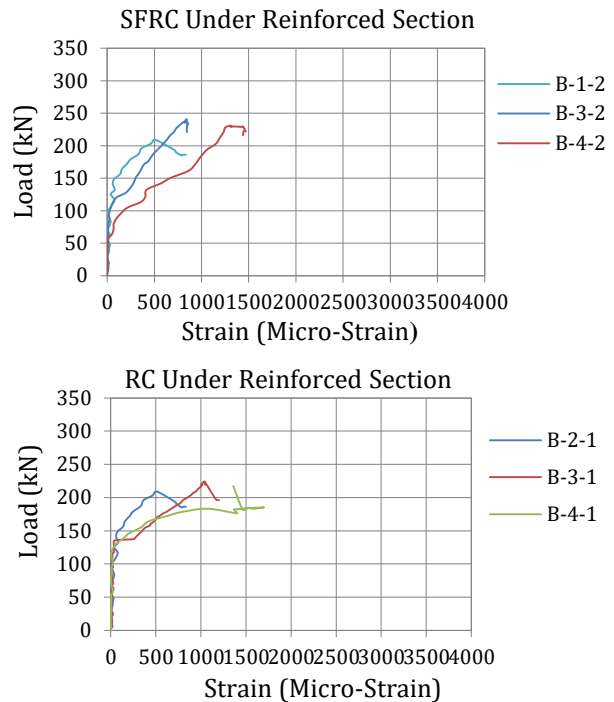


Fig.25 Load-Strain Curves of stirrup for under Reinforced Beams with and without Steel Fiber

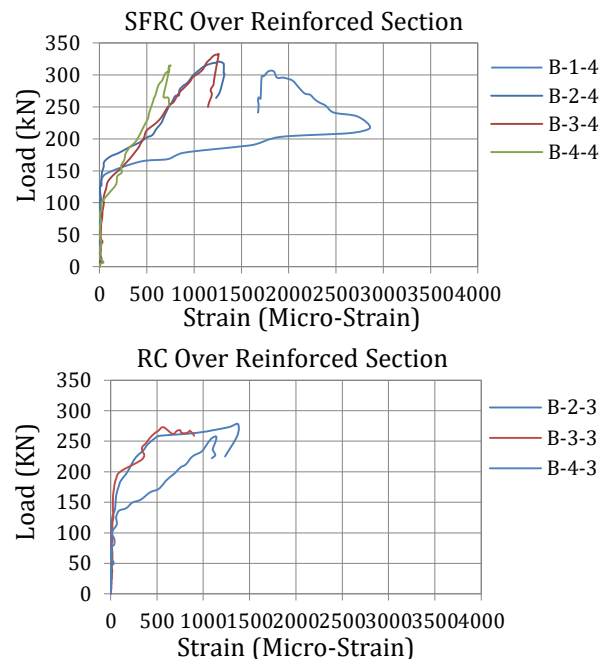


Fig.26 Load-Strain Curves of Stirrup for over Reinforced Beams with and without Steel Fiber

From above results it was found that:

1. The strain in tension bar increased for all hollow SFRC beams than RC hollow beams due to ability of steel fiber in transfer tensile force through cracks in tension zone and its multi axial effect.
2. The strain in stirrups in shear zone for hollow SFRC beams were still in close value to of hollow RC beams where the steel fiber at the diagonal cracks takes part of tensile force and reduce the stirrup stress.

5.5 Stiffness, Ductility Index and Absorbed Energy

Stiffness, ductility index and absorbed energy values for all tested beams are listed in Table 5. Initial stiffness is calculated as the slope of the first straight part of the load-deflection curve at cracking load value.

Table 5 Stiffness, Ductility Index and Absorbed Energy

Group	Beam	Stiffness kN/mm	Ductility Index μ_d %	Absorbed Energy kN.mm
G.1	B-1-2	21.81	5.60	3540.57
	B-1-4	24.93	6.93	6555.06
G.2	B-2-2	22.20	8.90	5259.12
	B-2-4	29.65	8.81	6811.35
G.3	B-3-2	27.82	10.88	6212.32
	B-3-4	32.08	9.47	6554.92
G.4	B-4-2	21.29	10.78	5746.54
	B-4-4	29.98	6.27	4247.62

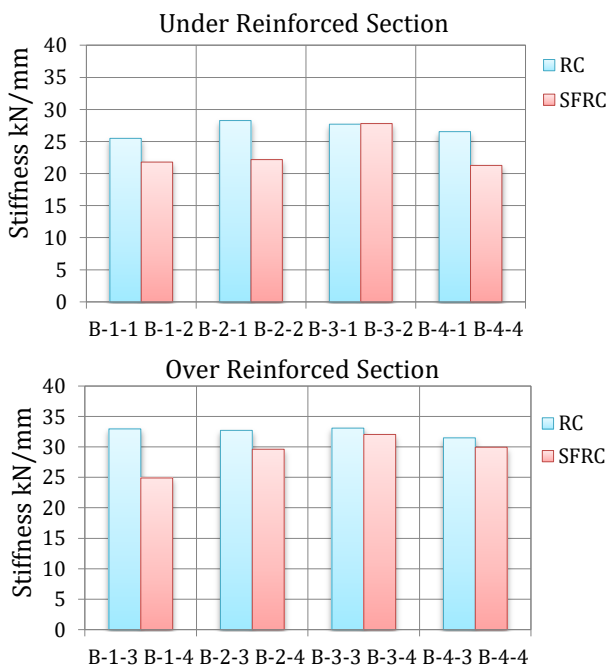


Fig.27 Stiffness of Hollow SFRC Beams and RC Beams with under and over Reinforced Sections

Ductility can be defined as the ability of material to absorb the inelastic energy without losing its loading capacity. Higher inelastic energy means higher ductility. So ductility index (μ_d) is calculated as the percentage of increase in elongation (from cracking stage to ultimate stage) relative to elongation at cracking stage:

$$\mu_d = \frac{\delta_{ul} - \delta_{cr}}{\delta_{cr}} \quad (10)$$

Where: δ_{ul} is mid span deflection at ultimate load and δ_{cr} is mid span deflection at cracking load.

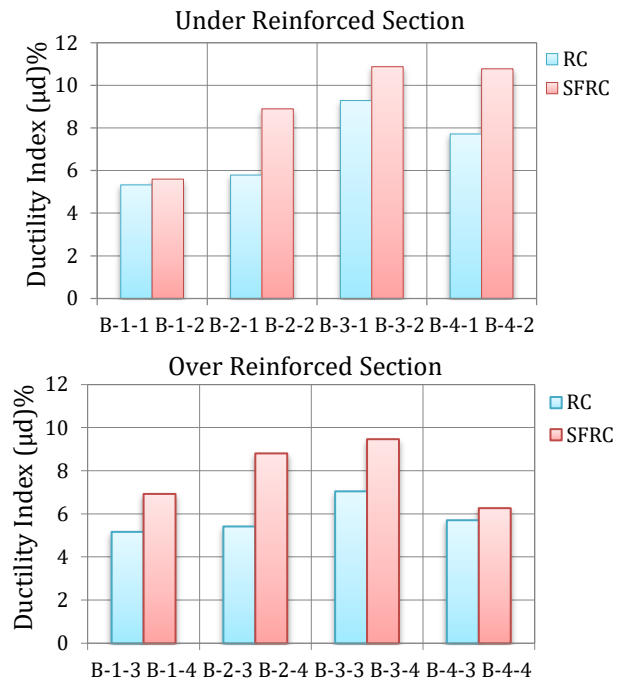


Fig.28 Ductility Index of Hollow SFRC Beams and RC Beams with under and over Reinforced Sections

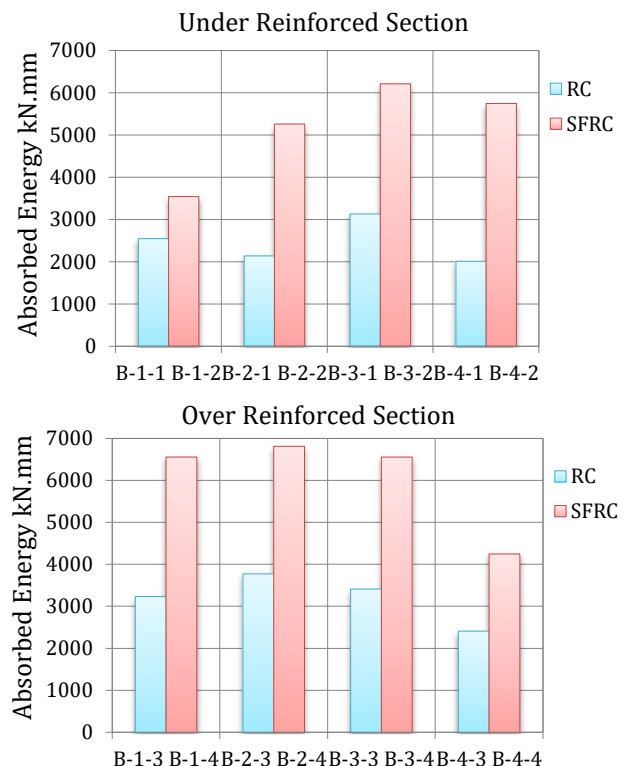


Fig.29 Absorbed Energy of Hollow SFRC Beams and RC Beams with under and over Reinforced Sections

The energy absorption based on displacement is Ability of a material to absorb energy prior to failure and calculated as the area under the load-deflection curve till failure load. By comparing results of tested hollow SFRC and hollow RC beams, it was found that:

1. For under reinforced section, initial stiffness of hollow SFRC beams decreased than hollow RC beams by value about 21.53%. But Ductility index and absorbed energy increased by value up to 39.64% and 186.25% respectively.
2. For over reinforced section, initial stiffness of hollow SFRC beams decreased than hollow RC beams by value about 24.43%. But Ductility index and absorbed energy increased by value up to 62.54% and 102.68% respectively.

6. Analytical Study

In this paper ANSYS 14.5 finite element analysis (FEA) software is used to simulate and analyze tested hollow SFRC beams. ANSYS allows engineers to save time and cost. For modeling element with ANSYS three stages must be followed:

- Pre-processing includes define the element type, Real constants, Material properties, Sections, Create the model and mapped mesh.
- Analysis solver by applying the boundary conditions, Loads and Solution.
- Post-processing of results like loads increment, deflections and stress contours.

6.1 Element Type and Real Constant

Table 6, Table 7 and Table 8 show used element and their real constrain to simulate hollow SFRC beams. Steel fibers were assumed as smeared reinforcement layers embedded in SOLID65 elements

Table 6 Element Type Used

Concrete	SOLID65
Steel Reinforcement	LINK180
PVC pipe	SHELL181
Loading & Supporting Steel Plates	SOLID 185

Table 7 Real Constant for SOLID65 Element with ($V_f = 0.75\%$)

1. Real Constants for SOLID65 with $V_f = 0.75\%$			
	for rebar 1	for rebar 2	for rebar 3
Material Number	5.00	5.00	5.00
Volume Ratio	0.0016	0.0016	0.0016
Orientation Angle	0.00	90.00	0.00
Orientation Angle	0.00	0.00	90.00

Table 8 Real Constant for Other Used Element

Real Constant	Element Type	Constant	
2. Main Reinforcement	LINK180	Cross- Sectional Area (mm ²)	201
		Initial strain (mm/mm)	0.00
3. Secondary Reinforcement	LINK180	Cross- Sectional Area (mm ²)	785
		Initial strain (mm/mm)	0.00
4. Stirrups	LINK180	Cross-Sectional Area (mm ²)	50.0
		Initial strain (mm/mm)	0.00

6.2 Material Properties and Define Section

To obtain accurate analysis, the following section shows parameters needed to define the material properties for used elements. SOLID65 element requires linear isotropic and multi-linear isotropic material properties to properly model concrete. Table 9 lists concrete properties. EX is the modulus of elasticity of the concrete and calculated based on the Egyptian Code equation (ECP-203-2017). PRXY is the Poisson's ratio (ν), it was assumed to be 0.2 for all specimens.

$$E_c = 4400 * \sqrt{F_{cu}} \text{ (MPa)} \tag{11}$$

As F_{cu} is the cube compressive strength without steel fiber. The multi-linear isotropic material uses the Von Mises failure criterion to define the failure of the concrete. The multi-linear stress-strain curve used to help with convergence of the nonlinear solution algorithm was obtained by the following equations (Desayi, 1964):

$$f = \frac{E_c * \epsilon}{1 + \left(\frac{\epsilon}{\epsilon_o}\right)^2} \tag{12}$$

$$\epsilon_o = \frac{2 * f_c'}{E_c} \tag{13}$$

ϵ_o is strain at the ultimate cylinder compressive strength f_c' and according to the (ECP-203-2017), it can be taken equal to $0.8F_{cu}$. Concrete material model in (ANSYS, SAS 2012) requires some constants be defined as shear transfer coefficient β which represents conditions of the crack face and determines the amount of shear transferred a cross the crack. The value of β ranges from (0.0 to 1.0), Uniaxial tensile cracking stress f_r and Uniaxial crushing stress f_c'

Table 9 Material Properties for Concrete

Linear Isotropic		Multi-Linear Isotropic		Concrete	
EX	24100	strain	Stress	β_o	0.30
PRXY	0.20	0.0003	7.60	β_e	0.90
		0.0006	13.35	f_r	3.32
		0.0009	18.15	f_c'	24.0
		0.0015	23.28		
		0.0018	24.00		
		0.002	24.00		
		0.003	24.00		

LINK180 element is used for modeling top and bottom steel reinforcement for all beams models and it requires linear isotropic and Bilinear Isotropic material properties, SOLID 185 element is used to model the loading and support plates to avoid stress concentration and it requires linear isotropic material properties also SHELL181 element requires linear

isotropic material properties as shown in Table 10. Then SHELL181 element needs to define sections by adding shell thickness and material properties used, as the thickness of 50mm PVC pipes is 2.2mm and thickness of 75mm PVC pipes is 2.4mm.

Table 10 Material Properties for Steel Reinforcement, Steel Plates, Steel Fiber and PVC pipe

2.LINK180	Linear Isotropic		Bilinear Isotropic	
	EX	2*10 ⁵	Yield Stress	400
	PRXY	0.30	Tang Mod	0.00
3.LINK180	Linear Isotropic		Bilinear Isotropic	
	EX	2*10 ⁵	Yield Stress	240
	PRXY	0.30	Tang Mod	0.00
4.SOLID 185	Linear Isotropic			
	EX	2*10 ⁵		
	PRXY	0.30		
5.Steel Fiber	Linear Isotropic		Bilinear Isotropic	
	EX	2*10 ⁵	Yield Stress	1050
	PRXY	0.30	Tang Mod	0.00
6. SHELL181	Linear Isotropic			
	EX	3300		
	PRXY	0.40		

Material model number 5 refers to steel fibers in the SOLID65 element. The area of reinforcement representing the fiber A_f is calculated based on the equation of (Soroushian and Lee, 1990):

$$A_f = \alpha V_f A_{ct} \tag{14}$$

Where: α orientation factor which is assumed as 0.64 for 2D and 3D orientation of fibers in beam and A_{ct} Cross-sectional area of a concrete element.

6.3 Modeling and Meshing

The beam, plates, and supports were modeled as volumes as in Figure30. The mesh is set up by creating square elements. The volume sweep command was used to mesh the steel plate, support and beam. This properly sets the width and length of elements in the plates to be consistent with the elements and nodes in the concrete portions of the model. The command (merge items) is used to merge separate entities that have the same location. The overall mesh is shown in Figure31.

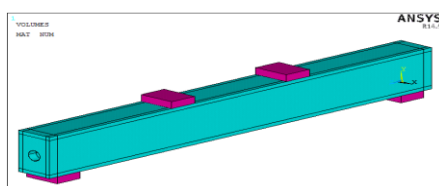


Fig.30 Volumes Created in ANSYS for Hollow Beam

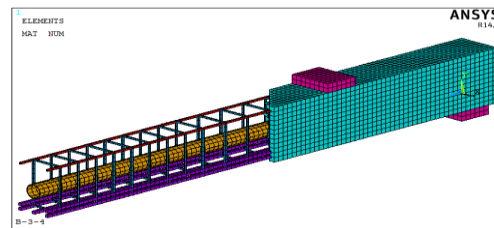


Fig.31 Meshing of Beam Model with PVC Pipe

6.4 Loads and Boundary Conditions

Displacement boundary conditions are required to constrain the model. Boundary conditions are applied where the supports and loadings exist. For hinged support a single line of nodes were given constraint in the UY, UX and UZ directions, and for roller support a single line of nodes were given constraint in the UY, UX. The force (P) is applied across the entire centerline of the plate as shown in Figure32.

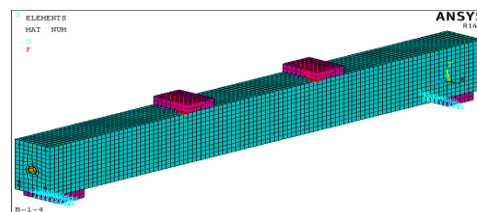


Fig.32 Boundary Conditions for Loading and Supporting Plates

6.5 Non Linear Solution

For these models, the static analysis type is chosen. In nonlinear analysis, the total applied load is divided into a series of load increments called load steps. At the completion of each incremental solution, the stiffness matrix of the model is adjusted to reflect nonlinear changes in structural stiffness before proceeding to the next load increment. The ANSYS program uses Newton-Raphson equilibrium iterations for updating the model stiffness (ANSYS, SAS 2012). The convergence tolerance limits were 0.50% for force checking and 5.00% for displacement checking to obtain convergence of the solutions. Failure for each model was identified when the program gives a message specifying that the model has a large deflection exceeding program displacement limitation.

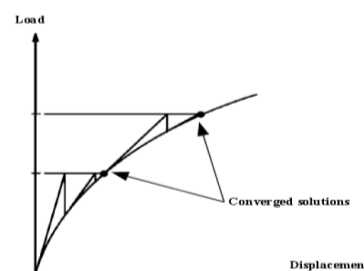


Fig.33 Newton-Raphson Iterative Solution

7. Analytical Study Results

Table 11 shows comparison between experimental and finite element results at failure stage to verify the accuracy of using finite element models.

Table 11 Comparison between Experimental and Analytical Results of Hollow SFRC Beams

Beam. No	P _{ul-Exp} (kN)	δ _{ul-Exp} (mm)	P _{ul-FEM} (kN)	δ _{ul-FEM} (mm)	P _{ul-Exp} /P _{ul-FEM}
B-1-2	221.9	16.92	219.6	20.30	1.01
B-1-4	305.7	18.26	277.3	8.95	1.10
B-2-2	218.1	16.33	218.3	18.67	1.00
B-2-4	320.7	18.62	271.0	8.95	1.18
B-3-2	241.0	18.22	216.1	17.50	1.11
B-3-4	332.6	19.03	283.8	11.13	1.17
B-4-2	231.0	14.86	214.7	18.50	1.07
B-4-4	314.7	15.38	274.0	13.08	1.15

From Table 11 it was found that, finite element ultimate load results are slightly smaller than experimental ultimate load with maximum difference (18.00%) this is due to:

- Finite element model does not have toughening mechanisms as in experimental beams like the grain bridging process, interlocking between the cracked faces, crack tips blunted by voids, and the crack branching process.
- Idealized stress-strain curve used for the steel was perfectly plastic stress-strain curve. Also for the concrete after the ultimate compressive so failure load in the finite element models were lower.

The deflection contours of the finite element model B-2-2 at the last converged load step is shown in Figure. 34 the contour lines for all models have the same shape but differ in the value.

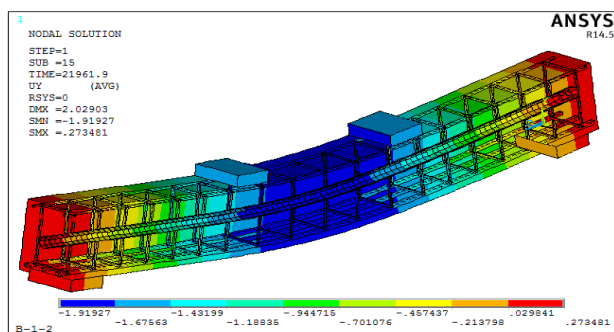


Fig.34 Deflection Contours for Hollow SFRC Beam Model B-1-2

7.1 Load Deflection Curves

Figure 35 and Figure 36 show the load deflection curves at mid span of finite element models with experimental tested beams for under reinforced section and over reinforced section respectively.

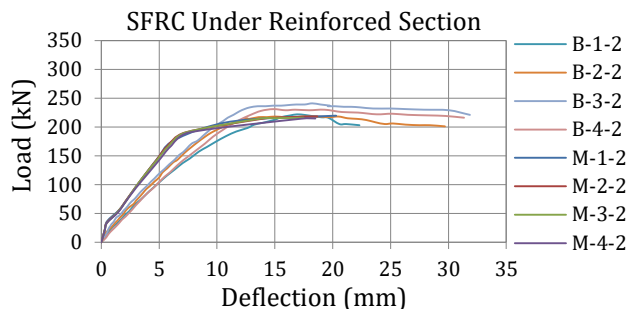


Fig.35 Load Deflection Curves of FE Models and Tested Beams for hollow SFRC under Reinforced Section

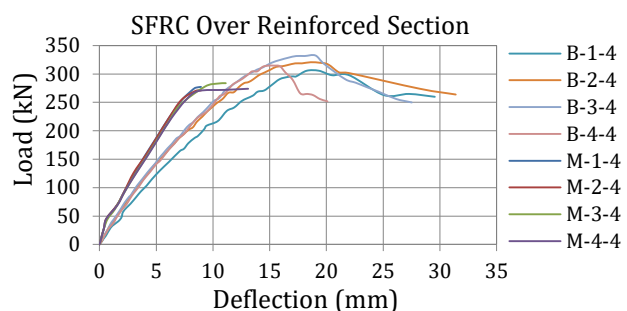


Fig.36 Load Deflection Curves of FE Models and Tested Beams for hollow SFRC under Reinforced Section

As shown in last two figures, Finite element model curves stiffer than the corresponding experimental curves and this is due to several factors:

- The finite element models do not include the micro-cracks produced by drying shrinkage in the concrete.
- The bond between the concrete and reinforcing steel is assumed to be perfect (no slip) but for the actual beams slip occurs.
- Inability of ANSYS to model the strain softening effect of concrete, the load deflection curve is only available till the ultimate load Then the program gives a message indicates failure of the model.

7.2 Cracking Pattern

A cracking sign in ANSYS represented by a circle appears when a principal tensile stress exceeds the ultimate tensile strength of the concrete. And it appears perpendicular to the direction of the principal stress and crushing is shown with an octahedron outline. The first crack at integration point is shown with a red circle outline, the second crack with a green outline, the third crack with a blue outline and closed cracks are shown with an X inside the circle as in Figure37.



Fig. 37 Symbols Used by ANSYS to Represent Cracking and Crushing

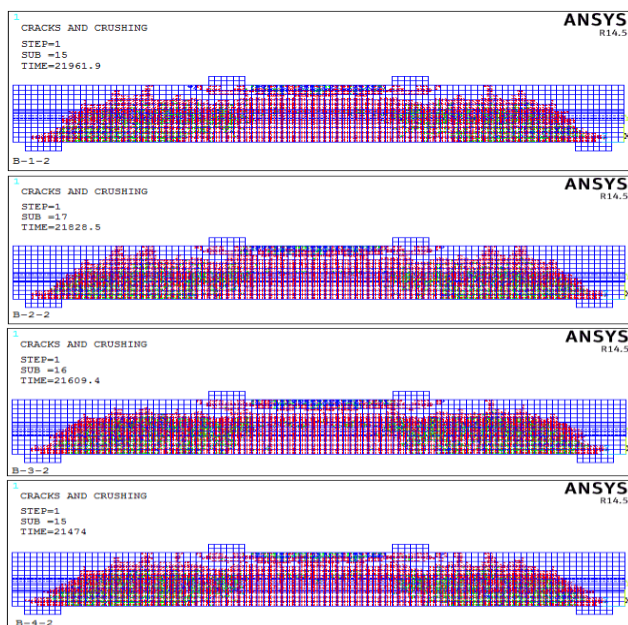


Fig. 38 Crack Pattern of under Reinforced Section

The cracking pattern was obtained using the crack/crushing plot option in ANSYS. Vector Mode plots must be turned on to view the cracks. Figure 38 and Figure 39 show evolutions of crack patterns developed for each hollow SFRC beam at the last converged loading step. The appearance of the cracks reflects the failure modes for the beams.

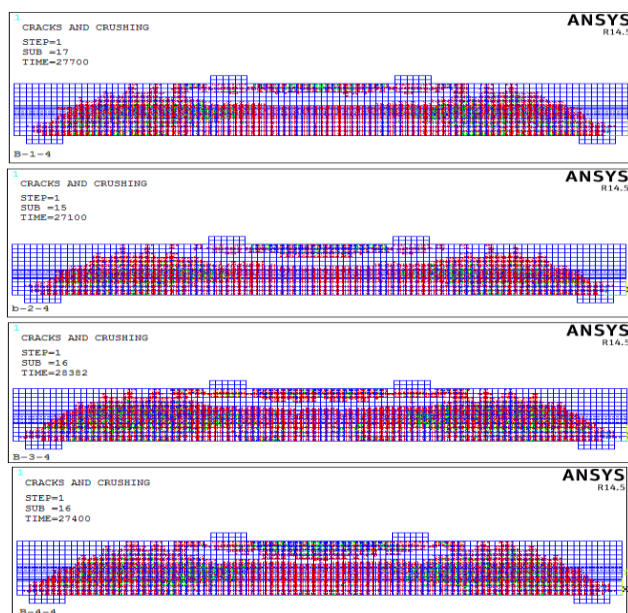


Fig. 39 Crack Pattern of over Reinforced Section

7.3 Stress Distribution

The finite element analysis provides stresses occurring at the integration points of solid elements. Maximum nodal stresses in concrete (plastic equivalent stress) and the nodal stresses in steel reinforcement (von-Mises stress) are obtained at the last converged load

step as in Figure 40 for beam model B-3-2. For the concrete once compressive stresses exceed the allowable compressive strength the failure will occur and this time recorded as failure time. For the steel when the equivalent stress exceeds the material yield stress, plastic deformation will occur. The maximum stress observed at bottom reinforcement in the mid-span of beam model.

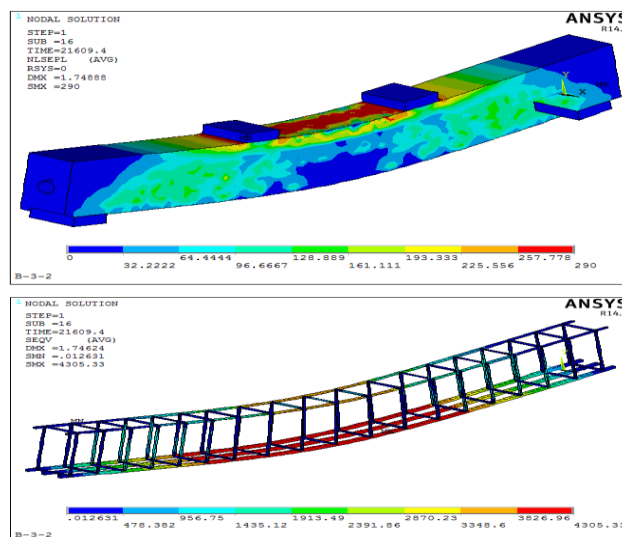


Fig.40 Stress in Concrete and Reinforcement for Model B-3-2

Conclusions

- 1) Adding steel fibers to concrete mix optimize the mechanical properties of all hollow beams through its ability to transfer tensile stress across crack surfaces of concrete so higher load carrying capacity achieved.
- 2) Adding steel fibers reduced the growth rate of the diagonal crack and increased deformation at failure so the brittleness of diagonal shear failure avoided and changed to more ductile one.
- 3) The load carrying capacity of under and over SFRC tested beams with inserted 50mm PVC pipe at two investigated location (160mm and 180mm) from the top increased by percentage about 3.64% to 17.58% than RC beams.
- 4) The load carrying capacity of under and over SFRC tested beams with inserted 75mm PVC pipe at two investigated location (160mm and 180mm) from the top increased by percentage about 7.58% to 24.73% than RC beams without steel fiber.
- 5) The addition of steel fiber develops higher strain in tension steel bars resulting in higher ductility.
- 6) For hollow under SFRC beams, ductility index and absorbed energy increased than hollow RC beams by value up to 39.64% and 186.25% respectively.
- 7) For hollow over SFRC beams, ductility index and absorbed energy increased than hollow RC beams by value up to 62.54% and 102.68% respectively.
- 8) The higher efficiency of steel fiber achieved with under reinforcement section, larger diameter and

lower location of PVC pipe as more cracks formed and more discrete steel fiber attribute in bridge and carry stresses crossing the crack faces, so a substantial ductility and absorbed energy can be attained.

9) Finite element ultimate load results were compatible to experimental ultimate load results with maximum difference (18.00%) also the load-deflection curves obtained from finite element are stiffer than that from the experimental data by value about (20.00%) this is due to ignoring concrete toughening mechanism.

References

- Clarke, Vollum and Swannell *et al*, (2007), Guidance for the Design of Steel Fiber Reinforced Concrete, *Report of a Concrete Society Working Group UK*, Technical Report No. 63
- Netra B. Karki, (2011), Flexural Behavior of Steel Fiber Reinforced Pre stressed Concrete Beams and Double Punch Test for Fiber Reinforced Concrete, *The University of Texas at Arlington in Partial Fulfillment for PhD*, pp. 15-21.
<http://hdl.handle.net/10106/11015>
- ACI 544-1R-96, (Reapproved 2002), State of the Art Report on Fiber Reinforced Concrete, *Report by ACI Committee 544*
- Kim, Kang and Lee, (2013), Influence of sand to coarse aggregate ratio on the interfacial bond strength of steel fibers in concrete for nuclear power plant. *Nuclear Engineering and Design*, 252, pp. 1-10
- Nasr Z, Hala M. & Amany S, (2019), Optimizing Behavior of Hollow Reinforced Concrete Beams, *PhD Dissertation, Civil Engineering Department, Helwan University*
- Johnston, C. D. (1974), Steel Fiber Reinforced Mortar and Concrete, A Review of Mechanical Properties, Fiber Reinforced Concrete, SP-44, *American Concrete Institute, Detroit*, pp. 127-142
- Thomas and Ramaswamy, (2007), Mechanical Properties of Steel Fiber Reinforced Concrete, *ASCE Journal of Materials in Civil Engineering*, Vol. 19, Issue 5, pp. 385-392
- Naaman, A.E, (2008), High Performance Fiber Reinforced Concrete, Chapter 3, pp. 91-153, for book edited by Caijun Shi and Y L Mo. titled, High Performance Construction Materials, Science and Applications, *World Scientific, Engineering material and Technological Needs*.
- Swamy, R. N., and Mangat, P. S. (1974), Theory for the Flexural Strength of Steel Fiber Reinforced Concrete, *Cement and Concrete Research*, Vol. 4, Issue 2, pp. 313-325
- Barr, B., (1987), the Fracture Characteristics of FRC Materials in Shear, *Fiber Reinforced Concrete Properties and Applications*, SP-105, *American Concrete Institute, Detroit*, pp. 27-53.
- Hai H. Dinh, (2009), Shear Behavior of Steel Fiber Reinforced Concrete Beams without Stirrup reinforcement, *A PhD Thesis, University of Michigan*
- ACI Committee 318, (2014), ACI 318-14, Building Code Requirements for Structural Concrete and Commentary, *American Concrete Institute, Farmington Hills, Michigan*.
- Gao J, Suqa W and Morino K (1997), Mechanical Properties of Steel Fiber Reinforced High Strength, Lightweight Concrete, *Cement and Concrete Composites* Vol. 19, no. 4, pp. 307-313
- Ashour, S. A., Wafa, F. F., & Kamal, M. I. (2000), Effect of the concrete compressive strength and tensile reinforcement ratio on the flexural behavior of fibrous concrete beams, *Engineering Structures*, Vol. 22, no. 9, pp. 1145-1158
- Henager C. H. & Doherty T.J., (1976), Analysis of Reinforced Fibrous Concrete Beams, *Proceedings, ASCE* Vol.102, ST1, pp. 177-188
- Cairns & Plizzari, (2004), Bond behavior of conventional reinforcement in fiber reinforced concrete, *In 6th RILEM Symposium of Fiber Reinforced Concretes (FRC)*, BEFIB2004, Varenna, Italy.
- ECP 203, (2017), Egyptian Code of Practice for Design and Construction of Concrete Structures, *Housing and Building National Research Center*, pp.4.3
- Desayi, P. and Krishnan, (1964), Equation for the Stress-Strain Curve of Concrete, *Journal of the American Concrete Institute*, Vol. 61, pp. 345-350
- ANSYS, "ANSYS Help", Release 14.5, Copyright (2012)
- Parviz Soroushian & Cha-Don Lee, (1990), Distribution and Orientation of Fibers in Steel Fiber Reinforced Concrete, *ACI Material Journal*, Vol. 87, Issue 5, pp. 433-439.